REPRODUCTION OF THE CAVITATING FLOWS PATTERNS IN SEVERAL NOZZLES GEOMETRIES BY USING CALIBRATED TURBULENCE AND CAVITATION MODELS

Miguel G. Coussirat[a], Flavio H. Moll[a] and Alfred Fontanals[b]

[a]*Grupo LAMA- Universidad Tecnológica Nacional-Facultad Regional Mendoza, Rodriguez 273, 5500 Mendoza, Argentina, miguel.caoussirat@frm.utn.edu.ar*

[b]*Departamento de Mecánica de Fluidos, Escola Enginyeria Barcelona Est, EEBE. Universitat Politècnica de Catalunya, España*

.

Keywords: cavitating flow, turbulence, orifices, nozzle-injectors, validation/calibration tasks.

Abstract. Cavitating flow is a complex phenomenon related with turbulent and multiphase flows with mass transfer between the liquid and gaseous phases. This flow is affected by several factors as surrounding pressure, the local state of the turbulence, the non-condensable dissolved gases concentration and others effects. To study this kind of flow, several numerical models have been developed and they are now available in commercial and in-house software. A numerical model for cavitating flows involves a multiphase model, including both mass transfer and turbulence submodels. Inside of a commercial or an in-house numerical code there are several options and possible combinations of these submodels. A selection of the more suitable combination from this broad offer is a difficult task, involving then a subsequent careful calibration of the models selected, due to the fact that the default values for the calibration parameters that have these submodels, are related to simple flow conditions, i.e., simple geometries and flows without any detachment. Under cavitation conditions, these conditions are not the common situation. This work deals with the enhancement of some previous results obtained that allow to say that it is possible to capture several cavitating flows characteristics, improving a 'standard' numerical (i.e., without any calibration) simulation by means of a detailed tuning of the production/dissipation coefficients present in the equations of the Eddy Viscosity Models for turbulence, and other parameters related to the two-phase state of the flow. The numerical results obtained were compared against experimental data for pressure, velocity and the structure of the two-phase cavity. It is demonstrated that a careful calibration of both the turbulence and the cavitation submodels used is of paramount importance, because there is a very close relation between the turbulence state of the flow and the cavitation inception/developing conditions. A suitable calibration work allows also diminish the mesh size, saving a lot of computational resources or the use of more sophisticated strategies for turbulence simulations (e.g., Large Eddy Simulations). Those are very expensive in terms of the necessary computational resources required. A more general conclusions than obtained in previous works are presented, because results for other different nozzles configurations were obtained.

1

1   INTRODUCTION

Cavitation is a complex phenomenon that appears in liquid flows when the hydrodynamic pressure falls out till values get nearer to the vapor pressure of the liquid, P_v. This low pressure provokes that the initial liquid flow becomes a two-phase flow (liquid-vapor bubbles), starting from the nucleation bubbles present due to the dissolves gasses contained in the liquid. If a nucleation bubble contains some gas, then the pressure in the bubble is the sum of the partial pressure of this gas P_G, and the vapor pressure. Hence the equilibrium pressure in the liquid is $P = P_v+P_G-2S/R$, where the critical tension is $2S/R-p_G$, S is the surface stress and R is the bubble radius. Thus, the presence of dissolved gases will decrease the potential tensile strength. Indeed, if the concentration of gas leads to sufficiently large values of P_G, the tensile strength is negative and the bubble will grow at liquid pressures greater than the vapor pressure, see details in Brennen 1995. The initiation of cavitation process by vaporization of the liquid therefore may require a negative stress existence, due to surface stress tension and other effects. However, the presence of undissolved gases particles, boundary layers, and the local turbulence state will modify and often mask a departure of the critical pressure from vapor pressure, Knapp et al., 1970. The pressure drop is related both to the hydrodynamic flow and to the physical properties of the fluid. Under this pressure drop condition, the vapor bubbles appear and grow in size. When this pressure drop goes down due to the local hydrodynamic flow conditions, a rising of the surrounding pressure appears, and now the pressure inside the bubbles is below of these surrounding field pressure values provoking that the bubbles collapse and condensate suddenly. If this collapse is near of the solid wall, the non-symmetrical distribution of the pressure field provokes high frequency and high intensity pressure pulses with a subsequent damage over the solid material (low and/or high cycles fatigue phenomenon). All the already described processes involve the complete cavitation phenomenon.

Steady and unsteady cavitating flows occur in many engineering systems from various applications. In most cases cavitation is an undesirable phenomenon (low performance and damage in materials) in other cases it is a useful application's tool. Some typical examples of low performance/damage in devices include cavitating flow into fuel injectors, liquid pumps, turbomachinery, hydrofoils, marine propellers, hydrostatic bearings and bio heart valves. On the other hand, examples of utility of this phenomenon are water-jet cavitation peening (WCP, for improving fatigue strength and wear resistance of metals), cavitating flow application used in a remarkable range of surgical and medical procedures, Coussirat et al., 2016a and Coussirat et al., 2016b and improvement of the spray characteristics in injectors, Sou et al., 2008a, and Sou et al., 2014.

In the specific case of injector fuel nozzles design, a designer must know details about the possible geometry to use and related to it, the conditions for the cavitation inception, its location place, dynamics, structure, and relation to the damage produced on the solid walls that interact with the fluid in order to control cavitation behavior. The structure and type of cavitation is of paramount importance for obtaining a good dispersion of the fuel at the nozzle outlet to improve its combustion. Results obtained show that the cavitation structure/type within the nozzle play a vital role on the spray pattern and the atomization phenomenon at the nozzle outlet. Several geometrical configurations can be seen for injectors (se details in Ganippa et al., 2004, Nurick et al., 2008, and Nurick 2011). Cases of in-line orifices (i.e., nozzles where the flow does not have any change in its direction) show a more symmetrical flow and spray pattern than inclined orifices. In this way, a suitable control of the cavitation stage could lead to a better spray structure, improving the subsequent combustion process. The structure of the cavity and its distribution within the nozzle is a key factor to be

considered in optimizing the spray pattern and to identify this situation several experimental have been made along the time, e.g. Nurick 1976, Chaves et al., 1995, Soteriou et al., 1999, Soteriou et al., 2001, Winklhofer et al., 2001, Ganippa et al., 2004, Sato et al., 2002, Dabiri et al., 2007, Sou et al., 2008a, Sou et al., 2008b, Nurick et al., 2008, Desantes et al., 2009, Sou et al., 2014 and Sou et al., 2015.

In these works a clear identification of the flow pattern under cavitation conditions is available, and the following classification is normally used normally: non-cavitating flow, incipient cavitation, developed or full cavitation and supercavitation, see Fig.1. Other existing condition, the flipping flow (i.e., separated flow), was only observed in some cases when the outlet is immersed in gas and for nozzle length/orifice diameter/width ratios (L/d, L/w) <10. A complete description of the aforementioned cases can be seen in Nurick 1976, Nurick et al., 2008, and Nurick 2011 and Duan et al., 2016.
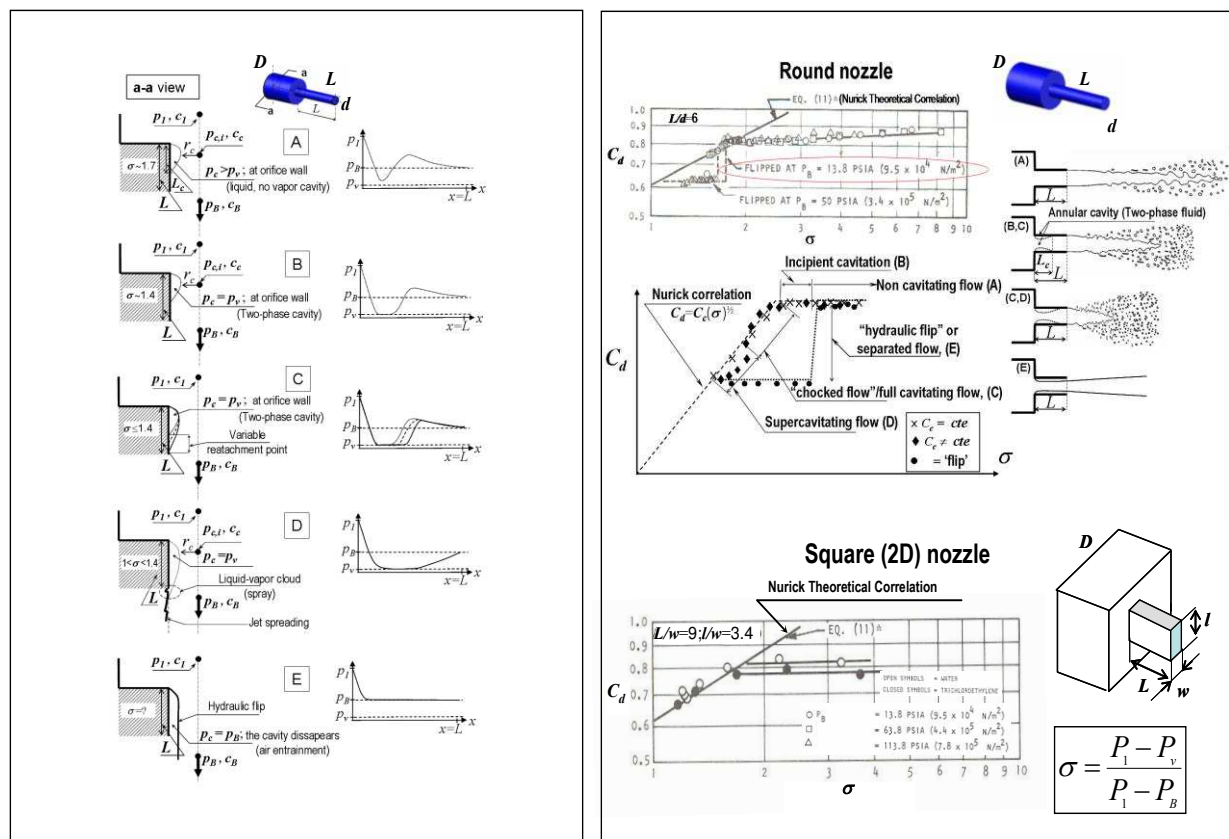

Fig.1: Cavitating flow categorization (stage/type), adapted from Nurick 1976 and Nurick 2011. **Left;** a-a nozzle views showing the four/five flow states in the nozzle: non-cavitation (A), incipient cavitation (B), full cavitation (chocked flow)/supercavitation (C-D) and hydraulic flip or flipping flow (E), and their pressure distribution along the orifice length. **Right:** Discharge coefficient, C_d vs cavitation number, σ (**Up:** for round nozzles, **Bottom:** for square nozzles). For round nozzles, only data for L/d=6 is shown here (having similar data for L/d=10 and L/d=20). For square nozzles, only data for l/w=3.4 is shown here (having also similar data for l/w=2.0 and l/w=8.0). **Notation:** c_I, Velocity inlet; c_B, Velocity outlet; d, Nozzle outlet diameter (round section); L, orifice length; L_c, Cavity length; l, nozzle height (square section nozzles); P_I, Inlet pressure; P_B, Outlet pressure; P_c, cavity pressure; P_v, Vapor pressure; w, nozzle outlet width (square nozzles); σ, Cavitation number.

In general for a suitable nozzle design it is necessary to know the cavitation condition that it has. Until now, this knowledge depends on a strong empiricism, because the 'theoretical

developments' available for cavitating flows study rely in semi-empiric models based in a set of representative cavitation (stage/type) coefficients. The majority of the actual knowledge is determined by an ad hoc definition of some non-dimensional coefficients for a certain cavitating flow stage.

Due to the strong difficulties for performing experiments in real Diesel injectors (technical issues and costs), Computational Fluid Dynamics (CFD) could be a powerful tool for nozzle design. In order to complement this empirical knowledge, from a decade ago till now several numerical models have been developed and incorporated in commercial or 'in-house' CFD codes. In spite of that, cavitating flows are still a big challenge for the numerical analysis using these codes, because cavitating flow modeling involves highly turbulent and two-phase flows. Normally, for cavitating flows, a Reynolds Averaged Navier Stokes equations plus an Eddy Viscosity Model (RANS+EVM equations) formulation for the mixture (liquid and vapor phases) is used for these simulations. Here, the mixture density, ρ, and the turbulent dynamic viscosity of the mixture, μ_t, 'are closed' (i.e., modeled) by cavitation and turbulence models respectively, being it commonly defined as a turbulent multi-phase flow modeling. Now, it is normal to find both several EVM models for turbulence and continuum models for two-phase flows in a CFD code. However, the implementation of models for cavitating flow is more recent and there is less work related to their validation and calibration. Then, the availability of simple and reliable CFD codes for both turbulence and cavitation models that allow decreasing the computing power is still an open issue due to the fact that both turbulence and cavitation phenomena offer several challenges for a suitable modeling by means of the available CFD codes.

It is known that turbulence affects cavitation inception since a nucleus may be found in the core of a vortex where the local pressure level is lower than a certain mean value of the pressure in the flow. Hence, the nucleus could cavitate when it might not do so under the influence of this mean pressure level. This fact points out that cavitation may alter the global pressure field by altering the location of flow separation and the induced variations of the local turbulence level; thus, turbulence may promote cavitation and vice versa. Although some details of these complicated viscous effects on cavitation inception were extensively examined by several authors in the past, the effects such as the interaction of turbulence and cavitation inception have been recently identified more clearly. To complete the list of those factors that may influence the cavitation inception, it is necessary to remark the effects of surface roughness and the turbulence level in the flow too. Therefore, it is not surprising that any individual effect be readily isolated from many of the experiments performed in the past Coussirat et al., 2016a.

Interaction of turbulence and cavitation has been studied both experimentally and numerically by many researchers on various application fields. For Diesel injectors and Venturis, results from several experimental databases are available, e.g., Nurick 1976, Winklhofer et al., 2001, Nurick et al., 2008, Sou et al., 2008a, Sou et al., 2008b and Nurick 2011. Unfortunately, for Diesel injectors cases, in general simultaneous measurements of velocity and pressures along the orifice are scarce yet, and detailed information related to the vapor fraction are neither available in these databases. Despite the aforementioned problems, these databases were extensively used in several CFD works, e.g., Gopalan et al., 2000, Yuan et al., 2001, Senocak, 2002, Senocak et al., 2002, Habchi et al., 2003, Vaidyanathan et al., 2003, Palau et al., 2004, Martynov et al., 2006, Goncalves et al., 2009, Darbandi et al., 2010, Duke et al., 2014, Congedo et al., 2015, Coussirat et al., 2016a, Coussirat et al., 2016b, Tseng et al., 2014, Naseri et al., 2015, Rodio et al., 2015, Koukouvinis et al., 2016 and Ghorbani et al., 2017. Some of these works also include CFD modeling for studying turbulence and cavitation interaction both for performing code validation/calibration tasks and for extending

the applicability of the available models. In this way, the numerical modeling has been improved considerably along the last 10-15 years, and for Diesel injectors design, current CFD applications have the capability for showing the impact of key design/operating variables on the discharge coefficient, C_d, on the contraction coefficient, C_c, and on the structure of the vapor cavity under cavitation conditions.

Concerning about the turbulence modeling, in general, the turbulence models employed in the cited works were EVMs, e.g., the Spalart and Allmaras, Standard, RNG and Realizable k-ε models, and Standard and SST k-ω and, in some cases, a linear pressure-strain Reynolds Stress Model, i.e., RSM, was used, (see full references of all these models in Coussirat et al., 2016a). It is highlighted that only in more recent works (e.g., Koukouvinis et al., 2016) both a RANS+EVMs formulation and others more sophisticated options, (e.g., the Wall-Adapting Local Eddy-Viscosity/Large Eddy Simulation, i.e., WALE/LES) were tested.

Regarding to the cavitation modeling, a barotropic model and several mixture models have been tested by the cited authors. In the mixture models used by them the phase change is governed by models based on the asymptotic Rayleigh-Plesset equation for the bubble dynamic, giving place to several formulations (e.g., Scherr et al., 2001, Singhal et al., 2002 and Zwart et al., 2004). In the case of mixture models testings, the results obtained by Palau et al., 2004, Coussirat et al., 2016a and Koukouvinis et al., 2016 also indicate that although the solved equations and phase change formulation are different in the cavitation models tested by them, both the cavity structure and the flow field predicted were very similar under the incipient cavitation condition.

Coming back to the turbulence modeling subject, and more in detail, it can be seen that the obtained results for round sections nozzles from Coussirat et al., 2016a and for square sections nozzles from Palau et al., 2004 and Koukouvinis et al., 2016 point out that all EVMs and RSM turbulence models without any calibration (i.e., using the default parameters for calibration) have failed to predict cavitation inception. It is believed that this could be due to their limitation to resolve adequately the flow pattern existing inside vortex cores, which is responsible for cavitation development in this particular flow configuration.
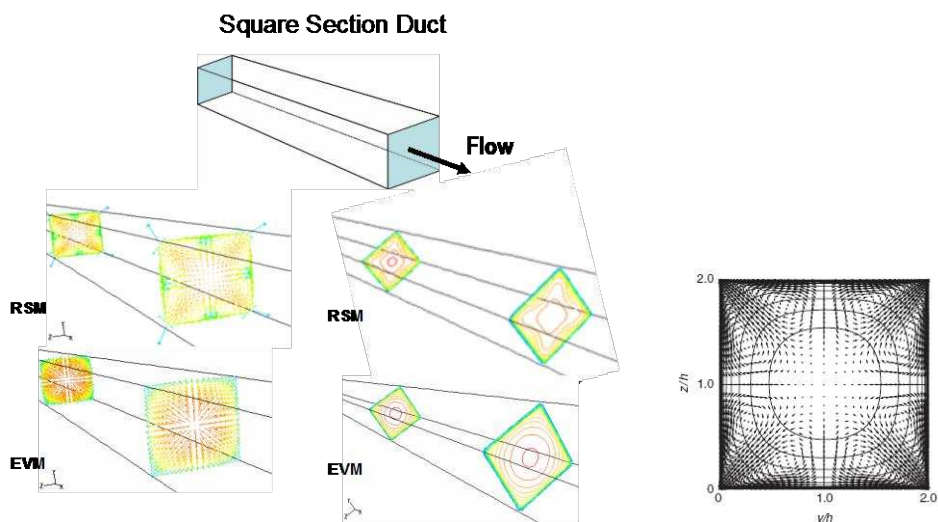

Fig.2: Representative flow field obtained by CFD simulations, using EVM and RSM in duct with square section. **Left:** Velocity field in the section. **Centre:** Velocity contours in the plane section. **Right:** Fully developed flow in a straight square duct at $Re_\tau \equiv 2hu^*/v = 600$; h = half of the square side; $u^* = (\tau_w/\rho)^{0.5}$; τ_w, wall stresses (taken from Durbin and Petterson 2001). The vectors show the secondary mean flow field.

It is also necessary to remark that the EVMs have the intrinsic problem for the prediction in a suitable way the shear stresses in ducts with square sections where the streamwise vorticity is generated by turbulent stresses. In these cases, the secondary flows due to the turbulence anisotropy are weaker than secondary flow due to the transverse pressure-gradients or the inertial forces, but this secondary flow substantially alters the characteristics of the whole flow field. Only by using a RSM this phenomenon could be captured, because a more real flow field is represented by RSM, see Fig.2. From a turbulence modeling perspective, this secondary flow prediction constitutes a demanding test, because a delicate imbalance between gradients of the Reynolds stress components is responsible for generating this secondary flow. This imbalance has to be accurately predicted for a suitable flow modeling in some cases.

The velocity vectors depicted in Fig.2 are an example of a secondary flow due the turbulence stresses imbalance. The primary flow is along the x axis. Flow in the $y - z$ plane would not be present under laminar conditions. It presence can be attributed to the streamwise vorticity generated by the turbulent stresses, (see more details in Durbin and Petterson 2001). Notice that there is none vorticity in the normal plane to the flow when an EVM is used. This is a typical fail from EVM due to the assumption of a scalar character for the turbulent viscosity in this kind of turbulence models formulation.

Even if the aforemetioned calibration problems for EVM turbulence were solved, both incipient and developed cavitation could be predicted in detail only by using RSM or LES models in square sections nozzles, being this fact an added difficulty for a suitable modeling using an EVM, because it does not predict well in detail the turbulence stresses.

On the other hand, at developed cavitation conditions the use of a 'standard turbulence modeling' (i.e., EVM or RSM) may predict unrealistically high liquid tensions, so modifications or accurate calibration of these models could be essential. The conclusions presented in Gonçalvez et al., 2012, Naseri et al., 2015, Rodio et al., 2015 and Koukouvinis et al., 2016 allow saying that the formation of vapor due to cavitation affects the fluid flow and a mutual interaction exists between the bubbles dynamics and the turbulent oscillations.

Turbulence is modulated by cavitation, but the detailed mechanisms of the interaction between turbulent flows and cavitation have not yet been clearly revealed, especially for phenomena occurring at small scales. This modulation can form a basis for a Sub Grid Scale (SGS) model for cavitation in Large Eddy Simulation (LES). It has been shown that traditional RANS+EVMs simulations without any calibration overestimate the turbulence dynamic viscosity, μ_t, of the mixture in cavitation zones, preventing the development of a re-entrant jet motion and the cavity shedding pattern, yielding unnatural results. RANS+EVMs simulations, however, are computationally less expensive than LES although they can have significant shortcomings in modeling turbulent cavitating flows. Some examples in order to estimate the CPU cost for LES computational requirement for cavitating flow in Venturis and nozzles are given in Spalart, 2000, Sou et al., 2014, Coussirat et al., 2016a and Koukouvinis et al., 2016. Then, the computing resources required for such a large grid make the LES simulations practically unfeasible for industrial flow simulations. Hence, the optimization of EVMs for expanded categories of flows is still useful and a necessary option nowadays. At the moment, a great amount of the CFD research related to the turbulence consists of case-by-case examination and validation/calibration tasks of existing turbulence models for such specific problems.

A set of general conclusions can be argued from the analysis of all of the aforementioned works: 1) Cavitation modeling has reached a stage of maturity at which it can consistently identify many of the effects of nozzle design on cavitation, thus making a significant contribution to nozzle (and other hydraulic devices) performance and optimization; 2) Both for round and square section nozzles RANS+EVMs without any calibration can predict

cavitation with a reasonably acceptable accuracy in an operating condition with not so high pressure difference (incipient cavitation) or when the ratios length nozzle/representative dimension of the outlet section (i.e., L/d or L/w, see Fig.1) are large, whereas they fail in the cavitation stage predictions at higher pressure difference or lower L/d, L/w ratios; 3) It is clear that several of the aforementioned characteristics of an unsteady 3D flow are not captured by steady state simulations. But in many cases, a steady state simulation could show the main features of a cavitating flow into the orifice nozzle, leading to a more accurate initial design and saving a lot of CPU resources; 4) It was demonstrated that 2D and 3D simulations provided quite similar results in terms of mean quantities (e.g., the mean cavity structure, time-averaged pressure and velocity fields/profiles in some cases, despite the broadly known full 3D nature of turbulence for round and square nozzles (more details for square nozzles will be given in Section 3); 5) The role of the wall functions and the subsequent meshing for CFD computations must be carefully defined; 6) The results obtained are more sensitive to the fine tuning of the turbulence models than to the tuning of the cavitation models; 7) All the cavitation models tested give similar results when they are coupled with the same turbulence models; 8) VOF and mixture models give very similar results for all the cases tested.

Besides this set of general recommendations, the most important conclusion of this literature analysis is to recognize that the use of models for cavitation and turbulence requires the setting of several calibration parameters that provide the needed experimental information required by a CFD code for the fluid flow simulation. For the available cavitation models they are dependent on some calibration parameters, such as the static pressure at the inlet, the turbulence level and the number of bubbles (or undissolved gases concentration that is not usually provided by the experimental databases, etc.). All of these parameters are useful for fitting/calibration procedures using the experimental data available, but unfortunately, these experimental data are not ever available or not well measured, representing an important source of uncertainty.

On the other hand, when a RANS+EVM simulation is considered, the turbulence model coefficients introduce an additional variability that relies in similar arguments that the ones aforementioned related to cavitation modeling. In fact, the assumption of some values for these empirical coefficients remains someway arbitrary, and sometimes tuned for reducing the diferences between experiments and numerical solution, but without a carefully analysis based on the turbulence theory, being it a difficult issue.

These uncertainties stem from the difficulties encountered to control accurately experiments in cavitating flows. It is not an easy task to define or to measure the physical fluid/flow parameters (e.g., undissolved gases contained, density or viscosity, turbulence level, etc.) that influence the subsequent CFD modeling through the imposed boundary and initial conditions, and through the behavior of the turbulence and cavitation submodels, being these influenced by the selected values for the aforementioned parameters.

Then, when the CFD task starts, it is not always possible to define accurately the values of some of these parameters that control the numerical simulation both for the EVMs and for the cavitation models used, because they are not clearly given in the experiments or in the theory. For these reasons, it is crucial to consider this epistemic uncertainty (since it is due to a lack of knowledge) in the problem for providing a measure of the variability of the numerical solution, i.e., assessing the quality of the numerical prediction, being this fact of paramount importance in cavitating flows in order not only for determining a converged numerical solution but also to obtain a description of the variability of the solution with respect to the known uncertainties.

Thus, all of these facts are additional sources of uncertainty, and some works on the interaction between cavitation and turbulence taking into account a fine tuning of the

7

turbulence models have been done recently to gain insight into this problem, see e.g., Zwart et al., 2004, Congedo et al., 2015, Coussirat et al., 2016a and Coussirat et al., 2016b.

A fine tuning of turbulence models try to recover the particular issue that is the behavior of turbulence under cavitation conditions, because cavitation affects its production, convection and dissipation in some way. The default values set for the parameters that control these effects in an EVM were obtained by using results from experiments in simple flows without any detachment over simplified geometries where cavitation is not present. The majority of the aforementioned studies were related to round nozzles. In the present work, this sensitivity study was extended to other nozzle geometries including square section nozzles, enlarging the previous works results obtained by the authors of the present work. More specific details and references concerning turbulence and cavitation models used here can be seen in Coussirat et al., 2016a and Coussirat et al., 2016b.

Finally, it is highlighted that an accurate study of the behavior for the turbulence and cavitating flow models is necessary for a suitable prediction of the characteristics of the spray that goes out from the nozzle for cases of Diesel injectors design or other similar devices. The designer must identify the correct flow state into the nozzle/orifice because this state has a tremendous effect on the external spray. Until now, unfortunately there is no a well established theoretical framework to determine the flow into the nozzle/orifice, and designers must rely on semi-empirical models obtained from experimental data. The aforementioned flow/cavitation stage of the internal flow directly affects the C_d too, being this clearly observed in cases of chocked or hydraulic flip flow when the outlet of the liquid flow is immersed in a liquid medium or in a gas medium respectively, (see details in Soteriou et al., 1999, and Soteriou et al., 2001). Hence, and depending on the fluid conditions at the nozzle outlet, cavitation phenomenon in the orifice induces mass flow chocking or flipping when the pressure drop increases. For this reason, a reduction in C_d values is expected when the flow reaches this stage. Therefore, a suitable cavitating flow modeling will be necessary to capture the cavitation inception for a subsequent prediction of the full cavitation, chocked or flipping flow stages.

2   APPLIED METHODOLOGY

In general the EVMs used for turbulence modeling without any calibration underpredict the cavitation inception for a given upstream pressure for round nozzles with lower inlet/outlet sections and nozzle length/outlet diameter ratios ($D/d<3$ and $L/d<10$ respectively), where the flipping phenomenon appears almost at the same time as the cavitation inception. An extensive discussion of these facts was given in Coussirat et al., 2016a, Coussirat et al., 2016b. In this work the same methodology as in the previous works is applied for several nozzles configurations. These new configurations were defined by means of changes in the D/d and L/d ratios in round nozzles and adding nozzles with square sections. The experimental databases from Nurick 1976 and Sou et al., 2006 were used to define the cases setup and for checking the results obtained. Also, comparison against CFD results presented by Palau et al., 2004 and Koukouvinis et al., 2016 were made. Following the conclusions of the previous works from Coussirat, the selected turbulence models for using in this work were the two EVMs already checked, i.e., the Spalart Allmaras (SA) and the SST $k-\omega$ models (SST), because the idea of a possible performance improvement of these EVMs by means of modifications of their calibrations parameters is an interesting option that has not been fully explored yet, despite some work exploring this option has been carried out (e.g. see Bardow et al., 2008, Cappa et al., 2014, Coussirat et al., 2016a and Coussirat et al., 2016b). Also, the Standard $k-\varepsilon$ and a Reynolds Stress Modeling (RSM, from Launder et al., 1975) was used

here for the square section nozzles to analyse the already mentioned effects of shear stress anisotropy for these sections, see Fig.2.

Concerning to the EVMs parameters calibration, the previous works from Coussirat where the general structure of the EVMs transport equations (local and convective accelerations, production, transport, dissipation and source terms) was discussed were taken as reference too. There, it was pointed out that the majority of these terms have many calibration coefficients, normally tuned for simple attached flows and for simple geometries. Particularly, the impact of these model parameters (turbulence) in different classes of applications, is not fully understood, a fact already highlighted by Coussirat 2003. A systematic approach for assessing their impact involves optimization methods for CFD that allow quantitative model analyses by a rigorous comparison against experimental data. In relation to the turbulence parameter calibrations, the viewpoints stated in Bardow et al., 2008, help to gain insight in this subject, despite that this study involved a non-cavitating flow between plane plates and not so for orifices with cavitating flow. An extension of this kind of analysis to cases of cavitating flows in orifices was made by Cappa et al., 2014, Coussirat et al., 2016a and Coussirat et al., 2016b.

These works were carried out bearing in mind the following CFD results obtained by: 1) Coutier-Delgosha et al., 2003, showing that the CFD results can be improved by increasing the mixture by changes in the turbulent kinematic viscosity, v_t, in some way in the formulation of the Standard k-ε turbulence model. 2) Spalart and Allmaras et al., 1994, pointing out that in anisotropic flows, the v_t can increase only by modifying the effects of its production.

Taking into account that the turbulence instabilities could promote cavitation, the aforementioned ideas related to the behavior of the turbulence viscosity (i.e., μ_t, v_t) in boundary layer flows and the results from previous works related to calibration of EVMs, some calibration tasks of the coefficients related to the turbulence (coefficients affecting the v_t value, or coefficients affecting production/dissipation terms) was made. Here both round and square nozzles configurations were studied to check if it is possible an improvement of the CFD prediction of the cavitation inception stage for these nozzles.

The selected coefficients were: 1) For the SA model: C_{v1} and C_{b1} i.e., a 'global parameter' related directly to v_t and a 'local parameter' related to the value computed for the production of v_t, respectively; 2) For the SST k-ω model: β_i and β_∞^*, i.e., a 'global parameter' closely related to α^* that affects the computation of v_t, and a 'local parameter' correlated to the value of β^* responsible of the computed level of the dissipation of turbulent kinetic energy k, respectively. This selection relies in the previous results from Coussirat et al., 2016a and Coussirat et al., 2016b.

3 CFD MODELS DEFINED AND DISCUSSION OF THE RESULTS OBTAINED

A commercial code (ANSYS/FLUENT v12) was used for modeling a turbulent cavitating flow in several orifice injectors. The geometries selected for the CFD models were: 1) Round nozzles (axi-symmetrical 2D models): d=3.18 mm, D/d=12, L/d = 6, 10 and 20. These round nozzle data were selected to enlarge the studies already made in Coussirat et al., 2016a and Coussirat et al., 2016b; 2) Square nozzles (2D models): w=0.76 mm, D/w=2.54, L/w=9; 3) Square nozzles (full 3D models): w=0.76 mm, D/w=2.54, L/w=9, l/w=3.4; 4) Square nozzles (2D models): l=1mm, D/w=8, L/w=4 and l/w=0.25, see Fig.1 for details.

The geometries described in the items 1-3 were extracted from the Nurick, 1976 database and the last item from the Sou et al., 2006, Sou et al., 2008a and Sou et al., 2008b databases.

9

In order to define the boundary conditions for the CFD models setups, an analysis of the selected experimental databases for comparisons were made. Only mass flow measurements are available for the aforementioned round and square nozzles geometries from the Nurick's database. The mass flow was expressed ever by means of the discharge coefficient, $C_d = f(\dot{m}, A_B)$, see Eq.1. Nurick, 1976 also proposed a theoretical correlation, see also Eq.1, for computing values for the coefficient $C_d = f(\sigma)$ under cavitation conditions, being this correlation validated by means of comparisons against its own experimental data, being it broadly used for computing the C_d for nozzles and is very useful for pre-design. Here, this correlation is used for comparison against the numerical results obtained.

$$C_d = \frac{\dot{m}}{A_B \sqrt{2\rho_l(P_1 - P_B)}} = \underbrace{C_c \sqrt{\sigma}}_{Nurick\ correl.};\ \ \sigma = \frac{P_1 - P_v}{P_1 - P_B}, C_c = \left[0{,}62 + 0{,}38\left(\frac{d}{D}\right)^3\right] \quad (1)$$

Where: A_B, is the orifice outlet section; $\dot{m}$, is the mass flow rate; ρ_l, is the liquid phase density; P_1 and P_B, are the nozzle inlet and outlet pressure imposed respectively; C_c is the contraction coefficient and P_v, is a certain critical pressure, being this P_v value taken equal to the vapor pressure, despite that undissolved gas particles, boundary layers, and turbulence level could modify and often mask a certain departure of the critical pressure from the vapor pressure. A non-dimensional coefficient σ has been adopted as the parameter for comparison of vaporous cavitation events, Knapp et al., 1970.

Pressures at the wall and the cavity structure were measured by Nurick, but only for one round nozzle configuration (d=7.62 mm, L/d=5, D/d=2.88) already studied in previous works, see details in Coussirat el al., 2016a; these measured wall pressures were not used here. It is pointed out that both for the mass flow and for the wall pressures measured there is none information related to the probes/measurements uncertainties.
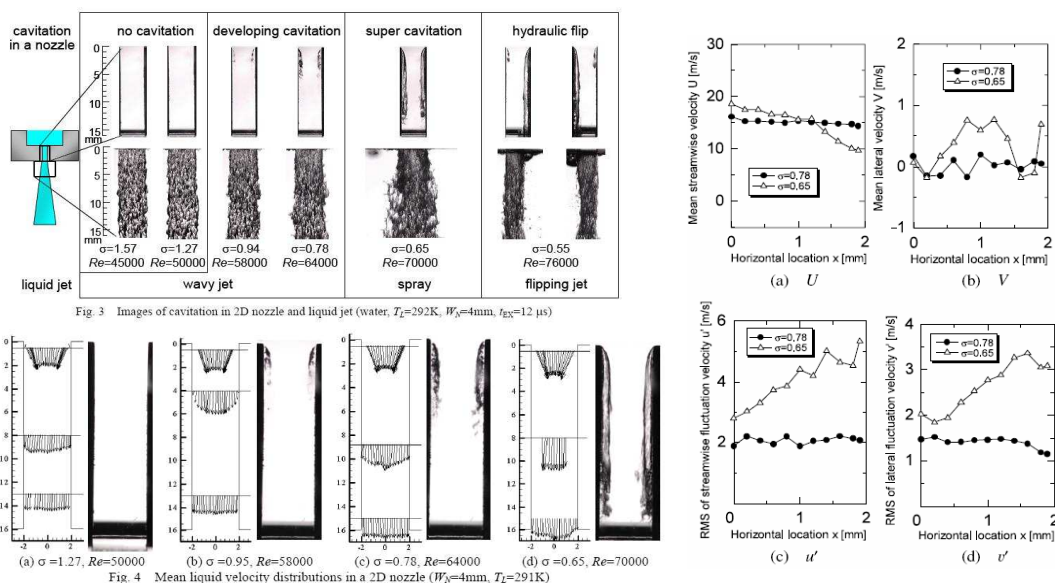

Fig. 3   Images of cavitation in 2D nozzle and liquid jet (water, T_L=292K, W_N=4mm, t_{EX}=12 µs)

Fig. 4   Mean liquid velocity distributions in a 2D nozzle (W_N=4mm, T_L=291K)

Fig.3: Experimental data for square nozzles, Sou et al., 2006, Sou et al., 2008a and Sou et al., 2008b:
Left, Top: Cavity structure. **Left, Bottom**: Velocity field in the nozzle measured by means of LDV technique.
Right: Mean velocity components (*U*, streamwise; *V*, transversal) profiles and its turbulent *rms* fluctuations
(*u′, v′*) in some positions (only y=15mm is shown here). **Notation:** *Re*, Reynolds number; σ, cavitation number,
Here, $\sigma = \sigma_{Sou} = (p_b - p_v)/(0.5\rho_l c_1)$; T_L, liquid temperature, W_N=w, nozzle width, Fig.1, t_{EX}, exposition time (photos).

For the square nozzles from the Sou et al., databases, there are measurements for: 1) The mean flow velocity at the outlet computed from the mass flow measured by means of flowmeters. The uncertainty in measured mass flow rate was less than 3.7 %; 2) The static pressure at a place 100 mm upstream of the nozzle (for some cases), measured by means of a Bourdon pressure gages; 3) The velocity profiles at some positions in the nozzle, measured by means of a Laser Doppler Velocimeter, LDV, device; 4) The concentration of oxygen dissolved in the water was measured using a dissolved oxygen probe. There is none information related to the probes/measurements uncertainties for the items 2-4.

Also, images for the vaporisation cavity structure when cavitation is present were taken using a digital camera and a flash lamp, see Fig.3, but without any information about the vapour fraction values in the cavity

Defining the CFD Setup

For the selected geometries the CFD estimations both for the flow separation and its reattachment, are strongly dependent on a correct prediction for the development of the near-wall turbulence and its instability, leading to the possibility to have an unsteady flow, giving place to unsteady CFD simulations, more expensive in terms of CPU requirements. To check this fact a detailed analysis of the experimental data was made.

In this line of analysis Nurick 1976 points out that a very stable cavity was observed in some cases, opening the possibility to perform steady flow simulations. This decision was reinforced by means of computing the Strouhal number, Sr=$L_\sigma \times (t \times c_\sigma)^{-1}$, where: L_σ is a characteristic length scale, t is a characteristic time scale of the unsteadiness and c_σ is a characteristic velocity scale. The problem now remains as far as how to define representative values for these scales. Some guidelines to define suitable values for these scales were taken from Dular et al., 2009, (see details and possibilities for these scales definition in Fig.2 and Fig.3 from Dular et al.) where it is pointed out that the mean length of the separated cloud just after the separation (shedding cloud) is an appropriate value for L_σ. But, there are numerous possible definitions for L_σ, and due to the fact that it is very hard to measure it precisely in many cases, a question remains here: which value for this mean length is the correct one?

When it is related to the cavitation structure and not to some other constant geometrical dimension, the only way to determine L_σ experimentally is by visual observation. Observations of incipient cavitation in experiments show that a reasonable value for L_σ is ~O(d) for injectors, (see details and references in Section 1).

The selection of a suitable value for c_σ is also difficult to address. The most accurate measure would be to use the re-entrant jet velocity at the closure of the attached cavity just before the cavitation cloud separates. A fair approximation, according to the potential flow theory, would be the velocity near the attached cavity closure point at the interface between the vapor structure and the pure liquid flow (see details in Dular et al., 2009).

Concerning the characteristic time of the unsteadiness t, it is known that cavitation unsteadiness is correlated with both high ($f \geq 5$–10 kHz) and low ($f \sim 100$ Hz) frequency noise signals, see details in Escaler et al., 2006 and Coussirat et al., 2016a. Therefore a characteristic value for $t = 1/f = 0.01$s is defined.

Afterwards, if all of these variables were known, a Sr number could be computed in a straightforward way, but as aforementioned, in the majority of the cases these ones are not known in advance. Instead of using the mean length of the separated cavitation cloud as L_σ and the re-entrant jet velocity as c_σ, variables that demand using costly visualization techniques, the most appropriate and also relatively easiest to determine are: the mean length

of the attached part of the cavity (of ~O(d) for injectors), and the corrected free stream velocity, $c_\sigma = c_B\sqrt{1+\sigma}$, Dular et al., 2009.

Assuming these variables as representatives of the unsteadiness, the Sr number was computed using L_σ=d=0.00318 m (D/d=12 cases) and the velocity c_σ of almost 20 m/s for a σ ~1.4, giving a c_B ~13 m/s. Visualization of the CFD results obtained here (not shown) confirms that the velocity in the interface of the cavity has similar values as the computed by using the aforementioned approach. Thus, a value of Sr ~3.2×10⁻³ was computed for the incipient cavitation stage, showing that the case with the geometry characterized by D/d=12, 6<L/d<20, could look like a steady phenomenon correlated with low shedding frequencies. On the other hand, if the same c_σ and t scales are considered, and L_σ =L=6×0.00318m for a full cavitation stage assumed, (i.e., a cavity with a L_c~L, being L the length of the orifice, see Fig.1), the computed value of Sr is now ~0.12×10⁻¹, being this value compatible with the values commonly observed for developed cavitation or supercavitation (intrinsically an unsteady phenomenon). Then, a steady state simulation is not representative for a subsequent nozzle design even though it could give some trends of its behavior, useful for design in these cases. Similar results were obtained for the Sr number (not shown) for the nozzles with square sections modelled in this work allowing the use of steady state CFD simulation in all cases to detect the incipient cavitation state.

Related to the selected geometry for modeling it is also necessary to highlight that experiments show that in cases with L/d ratios lower than 10, when the cavitation becomes developed, almost at the same time the flipping phenomenon appears, see Fig.1 and Fig.3. The flipping phenomenon is a detachment of the flow from the orifice wall without cavitation in a jet fashion suppressing the previously developed cavitation stage. This flipping condition is a severe restriction for CFD simulations, because the flow changes from cavitating flow to a free jet one, a completely different kind of fluid flow.

Therefore, a careful approximation to this condition is necessary in order to avoid the instability related to the change of the flow type. This fact is not taken into account by several authors found in the literature (see more details in Coussirat et al., 2016a).

Thus, over the selected geometries, the boundary conditions were defined in the same way as experiments, i.e., a pressure inlet condition P_I was imposed in cases from the Nurick database and a pressure inlet P_I or velocity inlet condition c_I was prescribed in cases from the Sou et al., databases. In all cases at the outlet a constant value for the pressure P_B was defined, see Table 1, Table 2 and Table 3.

These tables show the different combinations of turbulence models with the Singhal cavitation model that were used. Depending on the inlet pressure defined more or less combinations were used, highlighting the fact that for some inlet pressures there are less models combinations. There are two reasons for this shortcoming in models combinations in some cases: 1) To save CPU time, because slight differences in the results obtained were observed; 2) The models combinations start to show divergence due to the high pressure drop, showing a potential conflict between the pressures computed in the nozzle and the boundary condition imposed at the nozzle outlet.

In the cases of Table 3 the σ values were computed from Eq.2. It is remarked here that it is possible to find a relation between these two σ values (from Nurick, σ, and from Sou, σ_{Sou}), see also Eq.2.

$$\sigma_{sou} = \frac{p_B - p_v}{0,5\rho c_B^2}; \; \sigma_{Nurick} = \sigma = \frac{p_1 - p_v}{p_1 - p_B}; \; C_{d,Nurick} = C_c\sqrt{\sigma}; \; c_B = C_d\sqrt{\frac{2(p_1 - p_B)}{\rho}}; \sigma = \frac{1}{1 - C_c^2\sigma_{sou}} \quad (2)$$

Notice that each case in Table 1 and Table 2 was defined by setting a particular inlet pressure value, P_I selected from Nurick data, see Fig.1 while the outlet pressure P_B was set in 95,000 Pa in all cases. For each value of P_I defined, its associated σ value was computed by Eq.1. Instead, each case in Table 3 was defined by setting an inlet velocity value, c_I selected from the Sou databases, see Fig.3 while a value of P_B=95,000 Pa was set in all cases. For each value of c_I its associated σ and Reynolds number (Re) values were computed by means of the Eq.2 and $Re=c_Iw/v$ respectively.

Table 1: Round nozzles, D/d=12.0, L/d=6.0,10.0 and 20.0 (2D), from Nurick 1976: CFD cases modeled using the EVMs consigned in the table combined with the Singhal model.
Notation: A, SA; B, SST k–ω ; C, Standard k–ε

L/d	P_I[×10^{5}Pa]	1.20	1.50	1.64	1.85	2.02	2.10	2.30	2.50	2.75	3.00	3.75	5.00	6.50
	σ	4.66	2.66	2.32	2.02	1.85	1.79	1.68	1.59	1.51	1.45	1.33	1.22	1.16
6	EVMs used	AB	ABC	ABC	ABC	ABC	ABC	ABC	ABC		ABC	ABC		
10	EVMs used		ABC		ABC			ABC	ABC		ABC	ABC		
20	EVMs used		ABC		ABC	AB	AB	ABC	ABC	ABC	A	AB	AB	ABC

Table 2: Square nozzles, (D/w=2.54, L/d=9.0 (2D), and l/w=3.40 (3D), from Nurick 1976: CFD cases modeled using the EVMs consigned in the table combined with the Singhal model.
Notation: A, SA; B, SST k–ω ; C, Standard k–ε ; D, RSM.

l/w	P_I[×10^{5}Pa]	1.35	1.70	2.47	3.60	4.68	5.05
3.4	σ	3.27	2.22	1.60	1.34	1.24	1.22
	EVMs used	ABCD	ABCD	ABCD	ABCD	BCD	BCD

Table 3: Square nozzles, D/w=8.0, L/w=4.0, and l/w=4.0, (2D) from Sou et al., 2006, Sou et al., 2008a and Sou et al., 2008b databases. CFD cases modeled using the EVMs consigned in the table combined with the Singhal model. **Notation:** A, SA; B, SST k–ω, C, Standard k–ε; D, RSM.

l/w	c_I[m/s]	11.25	12.50	14.50	16.00	17.00	17.50	19.00	19.50
	σ	1.57	1.27	0.94	0.78	0.69	0.65	0.55	0.52
4.0	Re [×10^4]	4.50	5.00	5.80	6.40	6.80	7.00	7.60	7.80
	EVMs used	ABCD	ABCD	ABCD	ABCD	BCD	BCD	CD	CD

For defining the mesh size, the sensitivity mesh analysis (i.e., comparison of CFD results between several size meshes, and differences in results obtained between 2D and 3D cases) already performed in Coussirat et al., 2016a was used as reference. The meshes defined were: 1) For the Nurick 2D case axi-symmetrical, D/d=12 nozzles, Table 1: structured with quadrilateral cells for L/d=6, (21,000 cells); L/d=10, (26,000 cells) and L/d=20, (34,000 cells); 2) For the Nurick 2D case, D/w=2.54 square nozzle, Table 2: non-structured with quadrilateral cells for L/w=9.0, (23,000 cells). 3) For the Nurick 3D case D/w=2.54, l/w=3.40 square nozzle, Table 2: non-structured with hexahedral cells for L/w=9.0 (320,000 cells). 4) For the Sou et al., 2D case, D/w=8.0, l/w=4.0, Table 3: hybrid mesh quadrilateral/triangular cells for L/w=4.0 (16,000 cells).

In all the cases modeled the cell size near the wall (at the nozzle inlet zone) was computed in order to obtain values for y^+ <15. It is necessary to take into account that the grid convergence studies with the wall functions approach fail in some cases because the wall boundary condition is ill-posed.

Here, the inner limit was defined for a suitable application of the standard wall functions, i.e., at a value of y^+~11 (laminar sublayer), for a well-posed 'wall function' boundary condition, although the selected turbulence models do not use this wall treatment, except the Standard k–ε and the RSM models. For these two latter models, a specific near-wall treatment

13

was selected (wall functions or simplified equations for boundary layer turbulence, see details in Ansys 2015).

This is a useful observation to save CPU resources for future applications in modeling complex 3D flow cases with turbulence models that need near-wall boundary conditions. Notice that to take into account the needed computational resources in 3D cases, a simple 180° evolving from the 2D geometry around the symmetry axis for the case of round nozzle, L/d=6, see Table 1, generates a 3D mesh of around $(3.0 - 4.0) \times 10^6$ cells for the already defined 2D mesh (see details in Coussirat et al., 2016a).

Concerning the selected models, in commercial CFD codes there are several possibilities for combining turbulence and cavitation models taking into account that two-phase flows can be modeled by means of the Mixture model or the Volume of Fluid (VOF) model (see details in Ansys 2015). By using the combinations of several turbulence and cavitation models, Coussirat et al., 2016a showed that the SA and the SST $k–\omega$ turbulence models together with the Singhal cavitation model proved to be the best combination of EVMs/cavitation models for nozzles. But, in this previous work, only the mixture model was used. A subsequent analysis of the performance of the Mixture and VOF models was performed by Coussirat et al., 2016b to check the differences between them, using both the Singhal et al., 2002 and Zwart et al., 2004 models for cavitation. Results obtained showed that there were negligible differences in all the cases modeled.

Finally, the following setups for a CFD modeling of the geometries selected were defined, including: 1) the use of the combination of SA, SST $k–\omega$ and Standard $k–\varepsilon$ turbulence models together with the Singhal cavitation model for round nozzles, see Table 1, and the RSM model also was used in square nozzles, see Table 2 and Table 3; 2) The selection of Second-Order Upwind schemes for all the equations (flow and turbulence), except for the vapor transport equation, where the 'QUICK' scheme was selected. The selection of the 'SIMPLE' scheme for the pressure–velocity coupling, see full details in Versteeg et al., 1996 and Ferziger et al., 2002; 3) The definition of values for the dissolved gases contained in the liquid phase into a range of $1.0 \ 10^{-5}$ - $1.5 \ 10^{-9}$ (in terms of mass fraction, 1ppm=10^{-6}) depending on the available information from experimental data; 4) The $O(10^{-5})$ imposition for the normalized residuals; 5) Prescription of double precision in the computed values.

Results Obtained for the selected cases

The CFD results obtained for the coefficient C_d (Nurick cases) are shown in Fig. 4 for round nozzles (Table 1) and Fig.5 for square nozzles (Table 2). On the other hand, the CFD results obtained for a square nozzle case (Sou cases) for the mean velocities, the structure of the cavity, the velocity field and comparison of values against experimental data for the components of the mean velocity at the outlet, when the σ coefficient is changed (Table 3) are shown in Table 4, Fig.6, Fig.7 and Fig.8 respectively.

For round nozzles with D/d=12, the results obtained show that C_d is underpredicted under non cavitation conditions in all L/d configurations when both the SA and the SST $k–\omega$ models combined with the Singhal model were used, see Fig.4 (it is highlighted that experiments do not give any information related to the measurements errors/uncertainties). On the other hand, the combination of the Standard $k–\varepsilon$ and the Singhal models gives lower C_d values than the others combinations. Also, the convergence for the last combination of models is very slow, requiring more iteration cycles. The converged solution was obtained when the normalised residuals go down by an $O(10^{-4}–10^{-5})$ and the inlet-outlet mass imbalance was of $O(10^{-5})$ too.
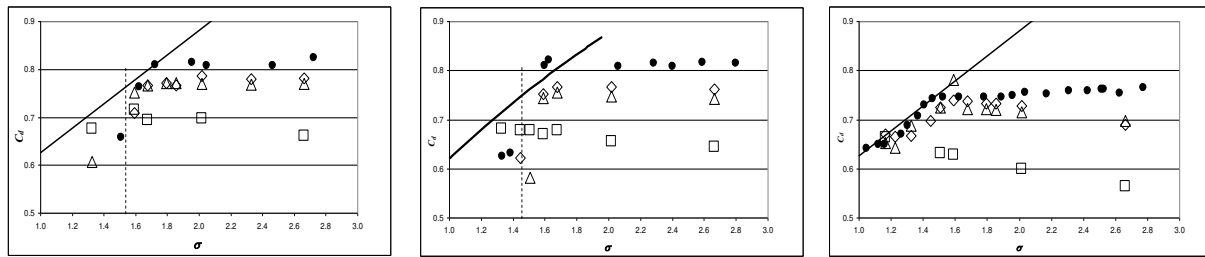
Fig.4: CFD results for C_d vs σ round nozzles: D/d=12, (Nurick 1976). **Left**: L/d=6, **Centre**: L/d=10; **Right**: L/d=20. **Notation**: D, inlet section diameter; d, outlet section diameter; L, nozzle length. — Nurick Theoretical correlation, Eq.1; ---Vertical line pointing out the σ value (Exp.) for the flipping condition with a sudden drop in C_d; • Experimental data from Nurick; CFD: □, Standard $k-\varepsilon$; ◇, SA; △, SST $k-\omega$.

Similar results were obtained for several round nozzles configurations and different operation conditions by other authors (e.g., Palau et al., 2004, Moll et al., 2011, Coussirat et al., 2016a). The cavitation inception is well predicted for the L/d=20 ratio (where the flipping is absent) when the SA and the SST $k-\omega$ models were used, giving the last model the best results. For L/d=6 and 10 ratios the flipping phenomenon appears almost at the same time as cavitation inception and the SST $k-\omega$ model gives the best results there.

It is highlighted that when the conditions imposed at the inlet (P_1) are correlated to the developed cavitation/flipping conditions as experiments show, the convergence starts to go down in the residuals obtained, but more important, the mass imbalance reached is only of $O(10^{-2})$, showing the necessity for other CFD strategy (e.g., unsteady VOF modeling). This fact was already observed by Coussirat et al., 2016a. Under the aforementioned condition both the SA and the SST $k-\omega$ models show certain convergence instability, being the SA model more sensitive and sometimes, the solution obtained with this model does not reach convergence. This instability in the convergence could due to the conflict that appears under the developed cavitation condition, between the pressure values predicted in zones nearer the nozzle outlet and the pressure boundary condition imposed at the outlet.
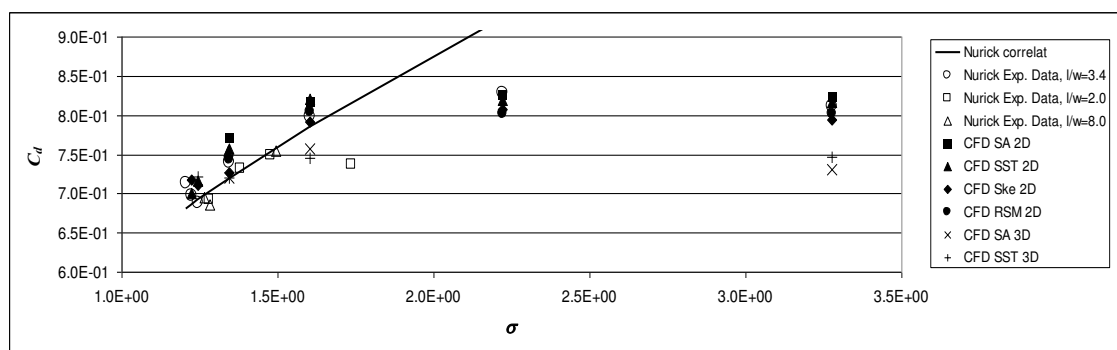

Fig.5 CFD results for C_d coefficient, square nozzles D/w=2.54, w=0.76mm, l/w=3.4 (3D), see Table 3. Experimental data, Nurick 1976. **Notation**: D, inlet section width; w, outlet section width; l, outlet section height; L, nozzle length; —, Nurick theoretical correlation, see Eq.1.

For square nozzles with D/w=2.54, both 2D and 3D CFD simulations were performed (see Table 2). For 3D cases a similar geometry as defined in Palau et al., 2004 was defined, but using more carefully the available nozzle geometry information, because several

15

mismatches/disagreements were found between the defined nozzle geometry from Palau et al., 2004 and the Nurick 1976 database.

The results obtained by 2D simulations show a slight undeprediction of the C_d in the non cavitating zone (σ >1.5), see Fig.5. All turbulence models give similar results (2D modeling) in this zone and the combination of the SA and Singhal models gives the best fitting here. Under incipient/developed cavitation the obtained results follow the experimental data and the Nurick correlation too, showing that it is possible to predict the C_d behavior under these conditions. The best fitting is provided by the SST $\boldsymbol{k-\omega}$ and the Standard $\boldsymbol{k-\varepsilon}$ models. This is an interesting result because the Standard $\boldsymbol{k-\varepsilon}$ performance for round nozzles was very poor, see Fig.4 (more details in Coussirat et al., 2016a).

Despite the improvement in its performance compated to the round nozzle cases, the Standard $\boldsymbol{k-\varepsilon}$ model needs more iteration cycles for reaching a converged solution. It was also observed that the convergence of SA and RSM models start to become unstable for incipient/developed cavitation conditions (σ >1.3), showing a clear rising in the mass imbalance. In all cases modeled the vapor fraction levels observed were probably low, but unfortunately, rhis fact cannot be confirmed because the experimental information related to the cavity structure in this case was not available.

It is remarked that despite the C_d values were well predicted, it is not a sufficient condition for a well predicted cavitation stage (and a cavity shape), an observation already pointed out in previous works (see details in Moll et al., 2011, Coussirat et al., 2016a and Coussirat et al., 2016b). This is a reason for the use of the data from Sou et al., 2006, where more detailed information concerning to the cavity structure than yhe one provided by Nurick 1976 and Nurick 2011 is given.

Also, in Fig.5 some C_d experimental measurements from Nurick for three values of the *l/w* ratio (full 3D experimental cases) were added. These results show an important dispersion of its values depending on the *l/w* ratio defined, showing the importance of the 3D effects. The CFD results obtained using the SA and the SST $\boldsymbol{k-\omega}$ models for a 3D geometry (only for the *l/w*=3.4 ratio) are shown too. Surprisingly, these models gave lower C_d values than experiemenal ones at σ >1.5, a fact that needs a more careful analysis. Under the incipient cavitation condition these models improve their performance and the C_d trend is closely followed by both models. Notice that for this geometry the flipping phenomenon was not reported by Nurick and also, the CFD results do not show this phenomenon.

Experiments, Sou 2006		SA		SST		Ske		RSM	
Mean Veloc. Outlet	Veloc. plenum	P1	Mean Veloc. Outlet	P1	Mean Veloc. Outlet	P1	Mean Veloc. Outlet	P1	Mean Veloc. Outlet
11.25	1.406	198514	11.31	197341	11.22	202064	11.25	*200129*	*11.29*
12.50	1.563	219566	12.53	220905	12.53	223293	12.51		
14.50	1.813	**279288**	**15.25**	277290	14.88	262448	14.50		
16.00	2.000	**336504**	**17.92**	336122	18.56	312741	16.65	*332343*	*18.37*
17.00	2.125			378661	24.36	355920	18.08		
17.50	2.188			401074	25.46	380347	23.52		
19.00	2.375					455639	27.21		
19.50	2.438								

Table 4: Experimental values from Sou databases, see Fig.3, and CFD results obtained for square nozzles (*l*=1 mm, *D/w*=8.0, *l/w*=0.25) for the mean velocity at the outlet, (c_B, [m/s]) and the inlet pressure P1 (P_1, [Pa] computed at the inlet. **Notation**: Veloc. plenum, c_1, [m/s]; numbers in **bold**: Divergence detected (imbalance of the net mass flow between inlet/outlet, residuals O($10^{-2} - 10^{-3}$); numbers in *italic*:1st discretization schemes (RSM); Captions: **RSM**, Reynolds Stress Model; **SA**, Spalart Allmaras; **Ske**, Standard $\boldsymbol{k-\varepsilon}$;**SST**, SST $\boldsymbol{k-\omega}$.

The necessity of a clearer analysis of the cavity structure represented by CFD appears and leads to the use of more recent databases where this information is available. The Sou et al., 2006, Sou et al., 2008a and Sou et al., 2008b databases could fulfil this requirement, see Fig.3, despite that pressures at the wall were not measured. In these databases, the inlet mass

flow was changed in order to obtain cavitating flow with different cavitation stages and cavity structures. The cavitation condition was defined by the cavitation number, σ, (σ_{Sou}) but now computed by the Eq.2. In this way, from the mass flow imposed, mean velocity values at the inlet were computed for several σ values, see Table 4. Using these values it was possible to define an inlet velocity condition (or mass flow inlet) and compute by CFD the mass flow rate in the nozzle to obtain both the pressure at the inlet and the mean velocity at the outlet.
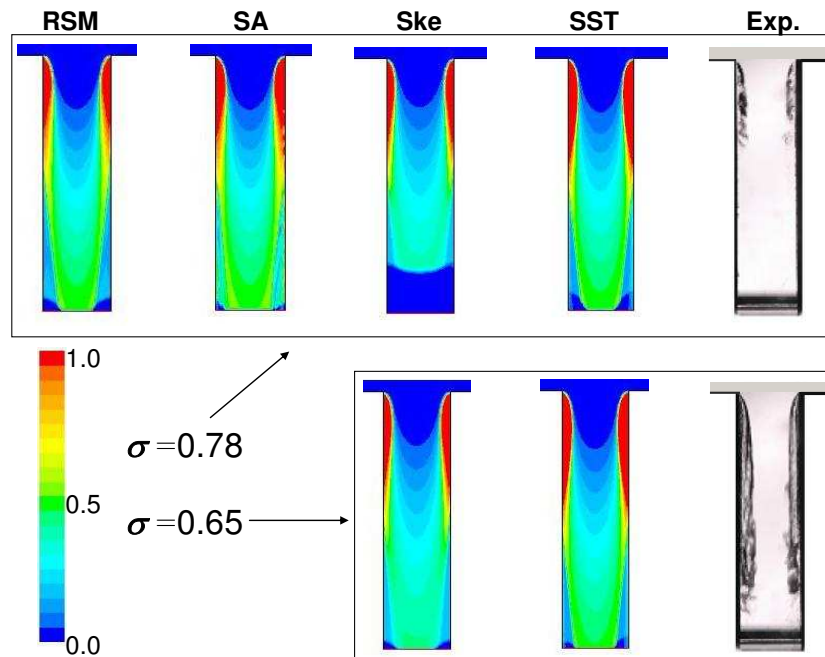

Fig 6: Comparison of CFD results obtained for the vapor fraction under two flow conditions, i.e., σ=0,78 and σ=0,65, see Table 3, Sou et al., 2006 case. **Notation**: 0.0 – 1.0 values in the scale are for vapor fraction; $\sigma = \sigma_{Sou}$, see Eq. 2; **RSM**, Reynolds Stress Model; **SA**, Spalart Allmaras; **Ske**, Standard $k-\varepsilon$; **SST**, SST $k-\omega$.

Experimental results show that the incipient cavitation starts at $\sigma \sim 0.94$, i.e., at c_B=14.50 m/s, reaching a stage of developed cavitation at $\sigma \sim 0.78$, (c_B=16.00 m/s) and the full cavitation stage at $\sigma \sim 0.65$, c_B=17.50 m/s.

The non-cavitation σ values, see pictures from Fig.3, are the values that allow defining the velocity values in the 1st and 2nd rows of the Table 4.

From the results shown in Table 4 it is possible to see that the Standard $k-\varepsilon$ model gives the best fitting for the outlet velocity, but this model also starts to give overpredicted c_B values at the developed cavitation stage (i.e., $\sigma \sim 0.78$, c_B=16.00 m/s). The SST $k-\omega$ model gives quite good adjustments until this condition too, but the other models tested give overpredicted c_B velocity values in all cases. The obtained vapor fraction field both for the developed cavitation ($\sigma \sim 0.78$, c_B=16.00 m/s) and for the full cavitation ($\sigma \sim 0.65$, c_B=17.50 m/s) stages computed by all turbulence models tested, can be seen in Fig.6.

For $\sigma \sim 0.65$ converged solutions were obtained only by means of the Standard $k-\varepsilon$ and the SST $k-\omega$ models. The results obtained for the cavity length are very similar as the ones predicted for the $\sigma \sim 0.78$ by these models and both models subpredict the cavity length. This situation is clearly correlated with the overprediction in the mean velocity at the nozzle outlet,

17

c_B. Notice that for $\sigma \sim 0.78$ there are not big differences in the cavity structure predicted for all models and its length is larger than the experimental length, being the one obtained by the Standard $\boldsymbol{k-\varepsilon}$ more similar as experiments show.

An intercomparison between the cavities predicted using the Standard $\boldsymbol{k-\varepsilon}$ and the SST $\boldsymbol{k-}$ $\boldsymbol{\omega}$ models for both σ values shows that there is a slight difference between both, being a bit larger for the lower σ value.

Finally, all CFD results obtained show some differences in the vapour fraction at the outlet. The more different vapour fraction pattern at the nozzle outlet was computed by the Standard $\boldsymbol{k-\varepsilon}$ model.

It is highligthed that in Table 4, the values marked in **bold** point out that some divergence was detected (rising in the net mass flow between inlet/outlet) for the SA model. On the other hand, values marked in italic point out that convergence was obtained by using 1st discretisation schemes for the RSM model. For this reason the comparison showed in Fig.6 does not include these models.

Fig 7 shows the obtained velocity field by means of the Standard $\boldsymbol{k-\varepsilon}$ model for developed cavitation, $\sigma \sim 0.78$, c_B=16.00 m/s and for full cavitation $\sigma \sim 0.65$, c_B=17.50 m/s. Also, the cavities obtained for both σ were added for clarity.

Notice that the velocity field is better predicted for $\sigma \sim 0.78$. The magnitude of the velocities is underpredicted in the $\sigma \sim 0.65$ case, in spite of the fact that the mean velocity value computed at the outlet (c_B) is higher than the experimental one, see Table 4. A reason of that could be the underprediction of the cavity length that leads to a different configuration of the velocity profiles nearer the nozzle outlet.

Unfortunately the experimental values for the cavity vapour fraction are not available for a better comparison, and in general only the structure of the cavity can be compared.
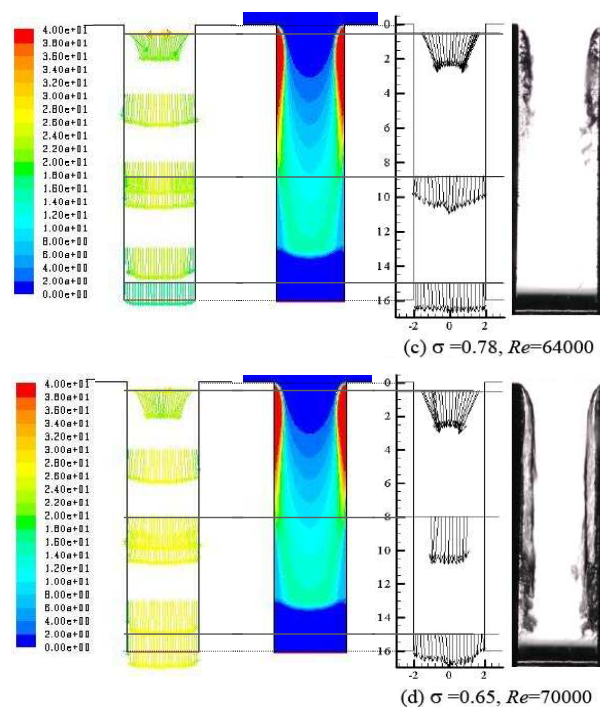

(c) σ =0.78, *Re*=64000

(d) σ =0.65, *Re*=70000

Fig 7: Comparison of CFD results obtained by using the Standard $\boldsymbol{k-\varepsilon}$ model for the vapor fraction and the velocity fields, under two flow conditions, i.e., σ =0.78 (**Up**) and σ =0.65 (**Bottom**), see Table 3. Experimental data are from Sou et al., 2006. **Notation**: $\sigma = \sigma_{Sou}$, see Eq. 2; *Re*: Reynolds number is based on c_B and w.

In order to clarify this fact a more detailed analysis of the CFD results for the velocities nearer the nozzle outlet was also made. Some comparisons between experiments and the CFD results obtained at the position y=15mm, (see Fig.3 and Fig.7) can be seen in Fig.8 for σ ~0.78, c_B=16.00 m/s and for σ ~0.65, c_B=17.50 m/s. Both streamwise, U_m, and lateral, V_m, components of the velocity were compared.
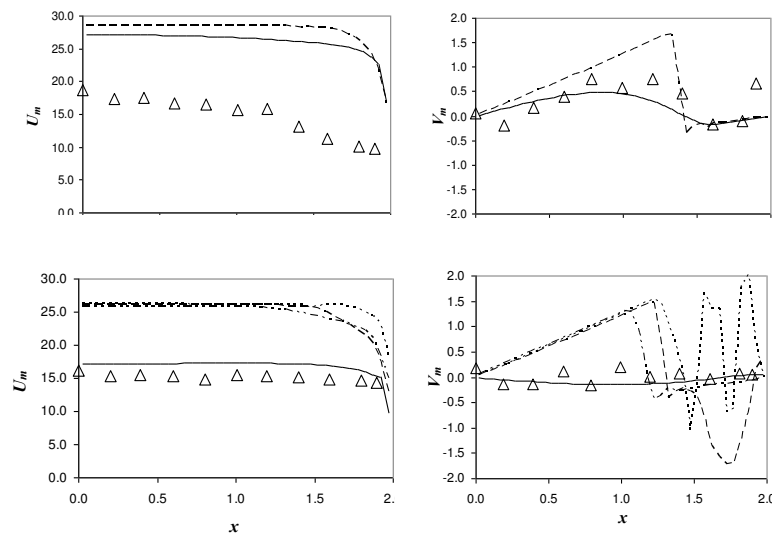

Fig. 8: CFD results, square nozzles , w=4.0 mm, D/w=8.0, l/w=0.25 (Sou databases, see Fig.3) for the mean velocity components (**Left**: Stremwise component, U_m; **Right**: Lateral component, V_m) at position y=15mm in the nozzle, and depending on the σ value. **Up** (**Left** and **Right**): σ=0.65; **Bottom** (**Left** and **Right**): σ=0.78. **Notation**: D, inlet section width; w, outlet section width; l, outlet section height; Δ, Experimental data from Sou for velocities. CFD results (2D): ——,Standard $k-\varepsilon$; ------, SST $k-\omega$; ······, SA; —– — , RSM.

For σ ~0.78, c_B=16.00 m/s only the Standard $k-\varepsilon$ model gives velocity profiles similar as the experimental values. All the others turbulence models overpredict these velocity values. Notice that strong oscillations appear in the computed V_m values for some of the turbulence models used. The reason for this behavior could be that the developed cavitation stage is not well predicted and this could affect the mean velocity computed. More research is necessary to clarify this fact.

Finally, following the ideas from Coussirat et al., 2016a and Coussirat et al., 2106b a preliminary sensitivity analysis of the cavity structure to the calibration coefficients for the SA and the SST $k-\omega$ models was also made for the Sou et al., 2006 case (w=4 mm, D/w=8.0, l/w=0.25). The preliminary results obtained by means of some changes in the default values for the coefficients selected, i.e. C_{v1}, C_{b1}, for the SA model; and β_∞^*, β_i, for the SST $k-\omega$ model respectively do not show a big sensitivity to these changes (not shown). A more extensive analysis is necessary to confirm these preliminary results, a goal of future work.

4 CONCLUSIONS

A set of CFD simulations for cavitating flow in several nozzles configurations has been carried out by using combinations of several turbulence models (SA, Standard $k-\varepsilon$, SST $k-\omega$ and RSM) and one for cavitating flow (Singhal).

For round nozzles with L/d >5, when incipient cavitation appears, a reasonably good adjustment for the coefficient C_d was obtained using the default values of the selected

19

calibration coefficients in the turbulence models. Previous works from Coussirat et al., 2016a showed that for L/d=5 or lower ratios, non-calibrated turbulence models fail to predict the C_d coefficient in some cases. Only by using the SA and the SST *k-ω* models, some suitable trends in C_d prediction were obtained under cavitation conditions near to the flipping flow condition when this condition could be appear (L/d=6 and L/d=10) confirming the conclusions already obtained in this previous work.

For square nozzles the use of EVMs with the default coefficients setting has a better behavior than for round nozzles. The quality of the CFD results obtained is also dependent on the nozzle length /outlet characteristic length ratio (i.e., L/w or L/l). The Standard *k−ε* model shows a good behavior in these cases showing suitable adjustments for the C_d coefficient and the best prediction of the mean values for velocities at the outlet in cases of square nozzles with low L/w ratios. Slight differences between 2D and 3D simulations were found for nozzles with high L/w ratios for the Nurick 1976 case.

A more detailed comparison (Sou et al., 2006 case) allows saying that despite that some clear differences among the mean velocity values at the outlet predicted by the turbulence models used, there are not big differences among the cavity structure predicted by all turbulence models. For the incipient cavitation condition the cavity structure predicted by CFD is larger than the experimental one, being the results obtained by the Standard *k−ε* closer to the measured cavity length. Instead, for developed cavitation the cavity length is underpredicted by all models tested.

Following the ideas of the previous works from Coussirat et al., 2016a and Coussirat et al., 2016b a preliminary sensitivity analysis of the calibration parameters provided by the developers of the SA and the SST *k-ω* models was carried out for square nozzles, but not big differences were found. It is remarked that the parameters selected for this sensitivity study are closely related to the turbulence viscosity, v_t, or its production or its dissipation. More research is necessary to clarify this fact being this subject a goal of future work.

5   AKNOWLDEDGEMENTS

REFERENCES

ANSYS Inc.,'ANSYS/FLUENT Soft.,', http://www.ansys.com/Industries/Academic/Tools/, 2015.
Bardow A, Bischof C and Bucker H, Sensitivity-Based Analysis of the k-ε Model for the Turbulent Flow Between Two Plates, *Chemical Engineering Science*, 63:4763 – 4775, 2008.
Brennen C, *Cavitation and Bubble Dynamics*, Oxford University Press, 1995.
Cappa F, Moll F, Coussirat M, Gandolfo E, Fontanals A, and Guardo A, Estudio de sensibilidad de parámetros de modelos en flujos cavitantes en régimen no estacionario, *ENIEF 2014* (in Spanish).
Chaves, H., Knapp, M., Kubitzek, A., Obermeier, F. and Schneider, T., Experimental Study of Cavitation in the Nozzle Hole of Diesel Injectors Using Transparent Nozzles, *SAE Tech.Paper*, No. 950290, pp 199–211, 1995.
Congedo, P., Goncalves, E. and Rodio, M., About the Uncertainty Quantification of Turbulence and Cavitation Models in Cavitating Flows Simulations*, Eur. J. Mech. B/Fluids* 53 pp. 190–204, 2015.
Coussirat M, Theoretical/Numerical Study of Flows with Strong Streamlines Curvature, *PhD*

Thesis, Universitat Politècnica de Catalunya, Spain, 2003.

Coussirat M, Moll F, Cappa F, and Fontanals A, Study of Available Turbulence and Cavitation Models to Reproduce Flow Patterns in Confined Flows , *ASME J. Fluids Eng.*, 138(9), 2016.

Coussirat M, Moll F, and Fontanals A, Capability of the Present Cavitating and Turbulence Models for Confined Flow Simulations, *ENIEF 2016* (in Spanish), 2016.

Coutier-Delgosha O, Fortes-Patella R, and Reboud J, Evaluation of the Turbulence Model Influence on the Numerical Simulation of Unsteady Cavitation, *ASME J. Fluids Eng.*, 42, pp. 527–548, 2003.

Darbandi, M., and Sadeghi, H., Numerical Simulation of Orifice Cavitating Flows Using Two-Fluid and Three-Fluid Cavitation Models, *Numer. Heat Transfer, Pt. A*, 58(6), pp. 505–526, 2010.

Dabiri S, Sirignano W and Joseph D, Cavitation in an Orifice Flow, *Physics of Fluids* 19, 2007.

Desantes J, Payri R, Salvador F, de la Morena J, Cavitation effects on spray characteristics in the near-nozzle field, *SAE Tech.Paper*, No. 09ICE-0151, 2009.

Duan L, Yuan S, Hub L, Yang W, Yu J and Xia X, Injection Performance and Cavitation Analysis of an Advanced 250 MPa Common Rail Diesel Injector, *Int. J. Heat Mass Transfer*, 93, pp. 388–397, 2016.

Dular M and Bachert R, The Issue of Strouhal Number Definition in Cavitating Flow, *Journal of Mechanical Engineering* 55(11), 666-674, 2009.

Duke, D., Kastengren, A., Swantek, A., Sovis, N., Fezzaa, K., Neroorkar, K. and Schmidt, D., Comparing Simulations and X-ray Measurements of a Cavitating Nozzle, *Proceedings of the ILASS-americas 26th Annual Conference on Liquid Atomization and Spray Systems*. Portland, USA, 2014.

Durbin P and Pettersson R, *Statistical Theory and Modeling for Turbulent Flows*, 1st ed,Wiley 2001.

Escaler X, Egusquiza E, Farhat M, Avellan F and Coussirat M, Detection of cavitation in hydraulic turbines, *Mechanical Systems and Signal Processing* 20 pp. 983–1007, 2006.

Franc J and Michel J, *Fundamentals of Cavitation,* Kluwer Academic Publishers, 2004.

Ganippa L, Bark G, Andersson S and Chomiak J, Cavitation: A Contributory Factor in the Transition From Symmetric to Asymmetric Jets in Cross-Flow Nozzles, *Exp. in Fluids* 36, pp. 627–634, 2004.

Ferziger J and Perić M, *Computational Methods for Fluid Dynamics,* 3rd ed, Springer 2002.

Ghorbani, M., Sadaghiani, A., Yidiz, M., and Kosar, A., Experimental and Numerical Investigations on Spray Structure Under the Effect of Cavitation Phenomenon in a Microchannel , *Journal of Mechanical Science and Technology* 31(1), pp. 235–247, 2017.

Gonçalves E and Decaix J, Wall Model and Mesh Influence Study for Partial Cavities, *Eur. J. Mech. B/Fluids* 31(1) pp.12–29, 2012.

Gopalan S, and Katz J, *Flow* Structure and Modeling Issues in the Closure Region of Attached Cavitation*, Phys. Fluids*, **12**(4), pp. 895-911, 2000.

Habchi C., Dumont, N. and Simonin, O., CAVIF: A 3D Code for the Modeling of Cavitating Flows in Diesel Injectors, *Paper N°95, DOI: 10.13140/2.1.3124.8324, ICLASS Conference*, Sorrento, Italy, 2003.

Knapp R, Daily J, and Hammit F, *Cavitation*, McGraw-Hill, New York, 1970.

Koukouvinis P., Naseri, H. and Gavaises M., Performance of Turbulence and Cavitation Models in Prediction of Incipient and Developed Cavitation, *International Journal of Engine Research*, 2016,

Launder G, Reece J and Rodi W, Progress in the Development of a Reynolds-Stress Turbulence Closure, *J. Fluid Mech.,* 68(3), pp. 537–566, 1975.

Martynov, S., Mason, D., and Heikal, R., Numerical Simulation of Cavitation Flows Based on Their Hydrodynamic Similarity, *Int. J. Engine Res.,* 7(3), pp. 283–296, 2006.

Moll F, H, Manuele D, Coussirat M, Guardo A, Fontanals A, Caracterización del tipo de cavitación mediante dinámica computacional de fluidos para posteriores aplicaciones al estudio

experimental del daño de cavitación, *ENIEF 2011*, (in Spanish), 2011.

Naseri, H., Koukouvinis, P., and M. Gavaises, Evaluation of Turbulence Models Performance in Predicting Incipient Cavitation in an Enlarged Step-Nozzle, *Journal of Physics: Conference Series*. Vol. 656. No. 1. IOP Publishing, 2015.

Nurick W, Orifice Cavitation and its Effect on Spray Mixing, *Journal of Fluids Engineering*, 98(2), pp 681-687, 1976.

Nurick W, Ohanian T, Talley D, Strakey P, The Impact of Manifold-To-Orifice Turning Angle on Sharp-Edge Orifice Flow Characteristics in Both Cavitation and Non-Cavitation Turbulent Flow Regimes, *J. Fluids Eng.* 130(12), 2008.

Nurick W, Flow Characteristics and Status of CFD Hydrodynamic Model Development in Sudden Contraction Manifold/Orifice Configurations, *Tech.Report, Nurick and Assoc.* Camarillo Ca., 2011,

Palau G, and Frankel S, Numerical Modeling of Cavitation Using Fluent: Validation and Parametric Studies, *AIAA Paper* No. 2004-2642, *34th AIAA Fluid Dynamics Conference and Exhibit*, Portland, Oregon, USA, 2004.

Rodio M, and Abgrall R, An Innovative Phase Transition Modeling for Reproducing Cavitation Through a Five-Equation Model and Theoretical Generalization to Six and Seven-Equation Models, *Int. J. Heat Mass Transfer,* 89, pp. 1386–1401, 2015.

Sato K and Saito Y, Unstable cavitation behavior in a circular-orifice flow, *JSME, Serie B*, 45(3) pp 638–645, 2002.

Senocak I, Computational Methodology for the Simulation of Turbulent Cavitating Flows, *Ph.D. Thesis,* University of Florida, USA, 2002.

Senocak I and Shyy W, Evaluation of Cavitation Models for Navier Stokes Computations, *Proceedings of FEDSM'02, 2002 ASME Fluids Division Summer Meeting*, 2002, Montreal, Quebec, Canada. 2002.

Singhal A, Athavale M, Li H, and Jiang Y, Mathematical Basis and Validation of Full Cavitation Model, *ASME J. Fluids Eng.*, 124(3), pp. 617–624, 2002.

Soteriou C, Andrews R and Smith M, Further Studies of Cavitation and Atomisation in Diesel Injector, *SAE Tech.Paper*, No. 1999-01-1486, pp 11–29, 1999.

Soteriou C, Andrews R, Torres N, Smith M and Kunkulagunta R, Through the Diesel Nozzle Hole—A Journey of Discovery, *14th Annual ILASS Americas Conference*, Dearborn, MI, 2001.

Sou A, Tomiyama A, Hosokawa S, Nigorikawa S and Maeda T, *Cavitation in a Two-Dimensional Nozzle and Liquid Jet Atomization (LDV Measurement of Liquid Velocity in a Nozzle),* , *JSME International Journal* Series B, Vol. 49, No. 4, 2006.

Sou A, Maulana M, Hosokawa S and Tomiyama A, Ligament Formation Induced by Cavitation in a Cylindrical Nozzle, *Journal of Fluid Science and Technology* 3(5) pp. 633–644, 2008.

Sou A, Maulana M, Isozaki K, Hosokawa S and Tomiyama A, Effects of Nozzle Geometry on Cavitation in Nozzles of Pressure Atomizers, *Journal of Fluid Science and Technology* 3(5) pp. 622–632, 2008.

Sou A, Biçer B, and Tomiyama A, Numerical Simulation of Incipient Cavitation Flow in a Nozzle of Fuel Injector, *Comput. Fluid*, 103, pp. 42–48, 2014.

Sou A, Minami S, Prasetya R, Pratama R, Moon S, Wada Y and Yokohata H, X-Ray Visualization of Cavitation in Nozzles with Various Sizes, *ICLASS 2015, 13th Triennial International Conference on Liquid Atomization and Spray Systems*, Tainan, Taiwan, August 23-27, 2015

Spalart P, and Allmaras R, A One-Equation Turbulence Model for Aerodynamic Flows, *Rech. Aeroespatiale*, 1, pp. 5–21, 1994.

Spalart P, Strategies for Turbulence Modelling and Simulations, *Int. J. Heat Fluid Flow* 21, pp. 252–263, 2000.

Vaidyanathan R, Senocak I, Wu J, and Shyy W, Sensitivity Evaluation of a Transport-Based Turbulent Cavitation Model, *Journal of Fluids Engineering,* 125, pp 447-458, 2003.

Tseng C, and Wang L, Investigations of Empirical Coefficients of Cavitation and Turbulence Model Through Steady and Unsteady Turbulent Cavitating Flows, *Comput. & Fluids* 103, pp. 262–274, 2014.

Versteeg H and Malalasekera W, *An Introduction to Computational Fluid Dynamics: The Finite Volume Method*, Addison-Wesley, 1996.

Winklhofer E., Kull E., Kelz E. and Morozov A, Comprehensive Hydraulic and Flow Field Documentation In Model Throttle Experiments Under Cavitation Conditions, *ILASS-Europe* 2001, Zurich, 2001.

Yuan, W., Sauer, J. and Schnerr, G., Modeling and Computation of Unsteady Cavitation flows in Injection Nozzles, *Mec. Ind*. 2, pp. 383–394, 2001.

Zwart P, Gerber A, Thabet B, A Two-Phase Flow Model for Predicting Cavitation Dynamics, *International Conference Multiphase Flow (ICMF),* Yokahama, 2004.